



Communication

A Novel Photoluminescent Ag/Cu Cluster Exhibits a Chromic Photoluminescence Response towards Volatile Organic Vapors

Wei Yang^{1,2}, Shengnan Hu¹, Yuwei Wang¹, Sisi Yan¹, Xiang-Qian Cao¹, Hong-Xi Li¹ , David James Young³ and Zhi-Gang Ren^{1,*} 

¹ Suzhou Key Laboratory of Novel Semiconductor-Optoelectronics Materials and Devices, College of Chemistry, Chemical Engineering and Materials Science, Soochow University, Suzhou 215123, China

² Faculty of Food Science and Technology, Suzhou Polytechnic Institute of Agriculture, Suzhou 215008, China

³ College of Engineering, Information Technology and Environment, Charles Darwin University, Darwin 0909, NT, Australia

* Correspondence: renzhigang@suda.edu.cn; Tel.: +86-512-65880328

Abstract: A new Ag/Cu bimetallic cluster $[Ag_{10}Cu_6(bdp\text{p}thi)_2(C\equiv CPh)_{12}(EtOH)_2](ClO_4)_4$ (**1**, *bdppthi* = *N,N'*-bis(diphenylphosphanylmethyl)-tetrahydroimidazole) exhibited strong phosphorescent (PL) emission at 644 nm upon excitation at 400 nm. Removal of the coordinated EtOH molecules in **1** resulted in derivative **1a**, which exhibited significant red-shifted emission at 678 nm. The structure and PL of **1** was restored on exposure to EtOH vapor. Cluster **1a** also exhibited a vapor-chromic PL response towards other common organic solvent vapors including acetone, MeOH and MeCN. A PMMA film of **1a** was developed as a reusable visible sensor for MeCN.

Keywords: photoluminescence material; vapor-chromic response; Ag/Cu complex; volatile organic vapor (VOC) detection



Citation: Yang, W.; Hu, S.; Wang, Y.; Yan, S.; Cao, X.-Q.; Li, H.-X.; Young, D.J.; Ren, Z.-G. A Novel Photoluminescent Ag/Cu Cluster Exhibits a Chromic Photoluminescence Response towards Volatile Organic Vapors. *Molecules* **2023**, *28*, 1257. <https://doi.org/10.3390/molecules28031257>

Academic Editors: Konstantin Brylev and Yann Molard

Received: 25 December 2022

Revised: 19 January 2023

Accepted: 24 January 2023

Published: 27 January 2023



Copyright: © 2023 by the authors. Licensee MDPI, Basel, Switzerland. This article is an open access article distributed under the terms and conditions of the Creative Commons Attribution (CC BY) license (<https://creativecommons.org/licenses/by/4.0/>).

1. Introduction

Volatile organic compounds (VOCs) are hazardous air pollutants. Some coordination compounds can serve as photoluminescent (PL) probes for VOCs with a rapid and reversible switching or chromic response [1–5]. Coinage metal complexes have been developed with useful photophysical properties such as sensitive and selective emission color changes under external stimuli [6–13]. Bimetallic Ag/Cu complexes have attracted considerable attention in this respect due to their low cost and rich luminescence behaviors. For example, Chen et al. have reported an Ag(I)-Cu(I) complex showing reversible vapor-chromic phosphorescence, with the emission changing from bright yellow to green in response to THF or $CHCl_3$ [14].

Vapor-chromic UV and PL responses of coordination compounds originate mostly from intramolecular structural distortion, such as the formation/disruption of metal–solvent bonds [15], molecular deformation [16,17] or conformational transformation [18,19]. The PL vapor-chromic response of metal complexes towards VOCs can be attributed to the interactions between the metal or their ligands and the VOC. In some cases, the small VOC molecules enter the lattice voids but do not participate in coordination bonds. There are only weak interactions, such as H-bonding, van der Waal's forces or $C-H\cdots\pi$ or $\pi\cdots\pi$ interactions between these 'free solvent molecules' and the main structure that partly affects the complex's energy levels [20–28]. In other cases, the VOC molecules coordinate with the metal ions to form metal–solvent bonds, which can significantly change the emission color or intensity [29–32]. For instance, Wang and co-workers have reported that the PL of an Au/Ag cluster reversibly shifted between green and yellow when the weakly ligated methanol molecules were removed or re-introduced [33].

Recently, we found that the strong emission of a Cu/Ag cluster $[Ag_{10}Cu_6(bdp\text{p}thi)_2(C\equiv CPh)_{12}(MeOH)_2(H_2O)](ClO_4)_4$ (**2**, *bdppthi* = *N,N'*-bis(diphenylphosphanylmethyl)-

tetrahydroimidazole) could be quenched by NH_3 , which enabled its use as a rapid, reversible and visual sensor [34]. During this quenching, the $\text{Ag}_{10}\text{Cu}_6$ cluster remained coordinated with MeOH and H_2O molecules, while the NH_3 only interacted with the MeOH ligands. Hence, we expected that the PL of this cluster would change when the MeOH and H_2O molecules were removed or replaced by other small organic molecules, such as VOCs, that could coordinate with the Ag/Cu cluster core directly. We therefore prepared a new cluster $[\text{Ag}_{10}\text{Cu}_6(\text{bdppthi})_2(\text{C}\equiv\text{CPh})_{12}(\text{EtOH})_2](\text{ClO}_4)_4$ (**1**), in which the solvates were replaced with EtOH. The luminescence of **1** significantly red-shifted on elimination of EtOH to produce **1a**, and was immediately restored upon exposure to EtOH. Other VOC vapors also resulted in a vapor-chromic PL response.

2. Results and Discussion

2.1. Synthesis and Characterization

2.1.1. Synthesis of **1**

The reaction of *N,N'*-bis(diphenylphosphanylmethyl)ethylene diamine (bdppeda), $[\text{Cu}(\text{MeCN})_4](\text{ClO}_4)$ and $\text{AgC}\equiv\text{CPh}$ (molar ratio 1:4:4) in $\text{CH}_2\text{Cl}_2/\text{EtOH}$ (Figure 1) produced bimetallic cluster **1** in 73% yield. This methodology was similar to that used in the synthesis of compound **2**, except for the solvent [34] and that the ligand bdppthi was generated in situ [35].

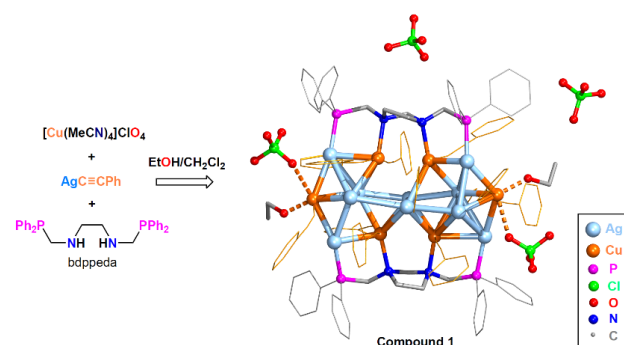


Figure 1. Synthesis and structure of **1**. The phenyl rings of $-\text{PPh}_2$ groups and $\text{C}\equiv\text{CPh}$ groups are plotted as gray and yellow hexagons. CH_2Cl_2 solvent molecules are omitted for clarity.

2.1.2. Single Crystal Structure of $\mathbf{1}\cdot 2\text{CH}_2\text{Cl}_2$

Single-crystal X-ray diffraction (SCXRD) of $\mathbf{1}\cdot 2\text{CH}_2\text{Cl}_2$ revealed that it crystallized in the monoclinic system $P2_1/n$ space group. The asymmetric unit contained one $[\text{Ag}_{10}\text{Cu}_6(\text{bdppthi})_2(\text{C}\equiv\text{CPh})_{12}(\text{EtOH})_2]^{4+}$ tetracation, four ClO_4^- anions and two CH_2Cl_2 solvent molecules. As shown in Figure 1, the $\text{Ag}_{10}\text{Cu}_6$ cluster core may be viewed as two smaller Ag_6Cu_3 units joined by sharing two Ag(I) cations. The two bdppthi ligands stabilized and connected the two Ag_6Cu_2 units through four Ag-P and four Cu-N bonds. Each Cu(I) atom was coordinated oppositely by two $\text{C}\equiv\text{CPh}$ anions. The average Ag-P, Cu-N and Cu-C bond lengths were 2.383(3), 2.271(9) and 1.915(13) Å, respectively. The $\text{Ag}_{10}\text{Cu}_6$ cores in compounds **1** and **2** were somewhat analogous. The Ag-Ag and Ag-Cu distances were in the range of 2.829–3.310 Å and 2.701–3.180 Å, respectively, indicating the presence of substantial metallophilic interactions [36]. Nevertheless, the metal–metal distances in **1** were slightly longer than those in **2**. The smallest Cu-Cu distance of 2.969(2) Å (between Cu2 and Cu3) was larger than the sum of the van der Waals radii of the two Cu atoms (2.80 Å), which ruled out the existence of Cu-Cu interactions and revealed that the $\text{Ag}_{10}\text{Cu}_6$ cores in **1** and **2** were different. The two Cu(I) atoms at the end of the $\text{Ag}_{10}\text{Cu}_6$ cluster core were further coordinated with the O atoms of two EtOH molecules (Cu1-O1, 2.043(8) Å; Cu4-O2, 2.031(9) Å). These two Cu-O (EtOH) bond lengths were slightly shorter than the Cu-O (MeOH) (2.1134(1) and 2.2071(1) Å) and Cu-O (H_2O) (2.1428(1) Å) interactions in **2**. These differences in bond lengths demonstrated that the metallophilic interactions in the $\text{Ag}_{10}\text{Cu}_6$ core were weakened when EtOH molecules were closely coordinated to the end

Cu ions. In addition, there were weak interactions between two of the ClO_4^- anions and these two Cu atoms: (Cu1-O5, 2.758(1) Å; Cu4-O9, 2.715(1) Å), while the other two ClO_4^- anions remained free.

2.1.3. Characterization of **1**

The CH_2Cl_2 molecules in $1 \cdot 2\text{CH}_2\text{Cl}_2$ readily escaped in air as evidenced by an absence of interaction in the solid-state structure. Thus, all other characterizations were performed on **1**. This cluster readily dissolved in common organic solvents such as CH_2Cl_2 , CHCl_3 , acetone, DMSO, DMF and MeCN, but was insoluble in Et_2O , hexane and H_2O . The elemental analysis of **1** was consistent with its molecular formula. The powder X-ray diffraction (PXRD) pattern of **1** correlated with the simulated spectra generated from the SCXRD data and was clearly different from that of **2** (Figure 2). The IR spectrum showed characteristic peaks at 2019 cm^{-1} for $\text{C}\equiv\text{C}$, 1082 cm^{-1} for ClO_4^- , and at 1483 , 1435 , 750 , 687 and 619 cm^{-1} for the $-\text{Ph}$ groups (Figure S1 (Supplementary Materials)). The positive-ion electrospray ion mass spectrometry (ESI-MS) of **1** (Figure S2) contained peaks attributed to $[\text{Ag}_2(\text{bdppthi})(\text{C}\equiv\text{CPh})]^+$ ($m/z = 785.03$) and $[\text{Ag}(\text{bdppthi})]^+$ ($m/z = 575.09$) cations and $\{[\text{Ag}_{10}\text{Cu}_4(\text{C}\equiv\text{CPh})_9(\text{H}_2\text{O})](\text{ClO}_4)_3 + e + \text{H}^+\}^{2+}$ ($m/z = 1278.89$) dications, indicating the structure of **1** partly decomposed in the ESI-MS environment.

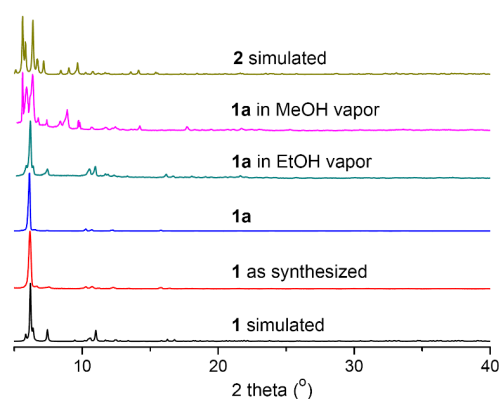


Figure 2. PXRD patterns of compound **1**, **1a** in air, **1a** in EtOH and MeOH vapors, and the simulated patterns of **1** and **2** from the SCXRD data.

2.1.4. Interconversions of **1** and **1a**

Thermogravimetric analysis (TGA) of **1** in a N_2 stream showed a weight loss of 2.2% between 120 and 150 °C, which matched the elimination of the two coordinated EtOH molecules (Calcd 2.24%) (Figure S3). We therefore treated **1** in vacuum by heating at 120 °C for 1 h and obtained its solventless derivative $[\text{Ag}_{10}\text{Cu}_6(\text{bdppthi})_2(\text{C}\equiv\text{CPh})_{12}](\text{ClO}_4)_4$ (**1a**). Cluster **1a** was less crystalline than **1** and not suitable for SCXRD analysis. The weak IR vibration at 3420 cm^{-1} attributed to the $-\text{OH}$ group of EtOH in **1** disappeared in **1a** (Figure S1). As shown in Figure 2, the PXRD pattern of **1a** was similar to that of **1**, indicating its cell parameter and major structure remained unchanged. The elimination of some weak peaks might be due to the elimination of the EtOH molecules. When **1a** was exposed to EtOH vapor for several minutes, the PXRD pattern fully recovered, indicating re-coordination of the EtOH molecules. However, when **1a** was treated with MeOH vapor, the PXRD pattern resembled that of compound **2**, indicating a phase-transition. This transition was reversible, so that desolvation of **2** and re-exposure to EtOH produced **1** quantitatively.

2.2. Photoluminescent Properties

2.2.1. Photoluminescent Properties of **1**

Upon excitation at 400 nm, crystals of **1** exhibited bright red emission at $\lambda_{\text{max}} = 644\text{ nm}$ (Figure 3) with a quantum yield (QY) of 10% at ambient temperature. The PL lifetime

(τ , excited at 373 nm) was 7.48 μ s. This relatively long lifetime and large Stokes shift (244 nm) suggested that this PL was a phosphorescent emission and likely arises from a metal cluster-centered triplet excited state modified by metal–metal interactions, mixed with a $[C\equiv CPh \rightarrow Ag_{10}Cu_6]^3LMCT$ transition [14,34]. The emission was not sensitive to excitation wavelengths, as the spectrum excited at 365 nm was similar to that excited at 400 nm except for a small intensity decay.

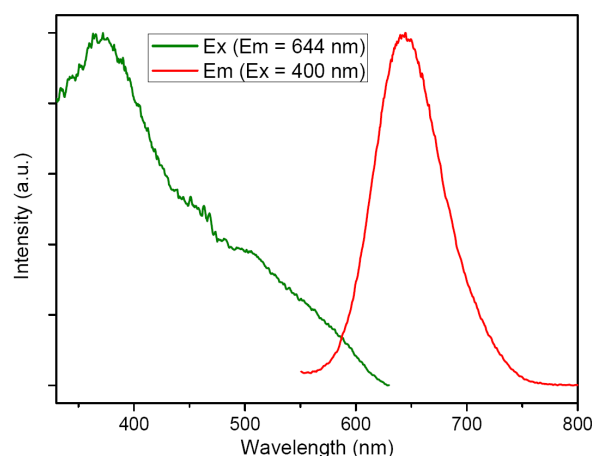


Figure 3. Excitation and emission spectra of **1** at ambient temperature.

2.2.2. Photoluminescent Properties of **1a** and Vapor-Chromic Responses toward Water and VOCs

Solid **1a** emitted at $\lambda_{max} = 678$ nm when excited at 400 nm (Figure 4). Compared to that of **1**, this emission exhibited a 34 nm red-shift, reduced intensity (QY = 6%), and a slightly prolonged lifetime ($\tau = 8.82$ μ s, excited at 373 nm). The emission of **1a** could be fully restored to that of **1** (644 nm) after exposure to EtOH vapor, and this process showed good repeatability over four cycles (Figure S4). The PXRD of **1a** remained steady during these cycles and for as long as one month later (Figure S5). We believe that during the interconversion of **1** and **1a**, the departure and re-coordination EtOH molecules from the Cu atoms affect the electron density of the $Ag_{10}Cu_6$ cluster center, which influences the $T1 \rightarrow S0$ energy band, and therefore the shifting of the emission wavelength and intensity arises.

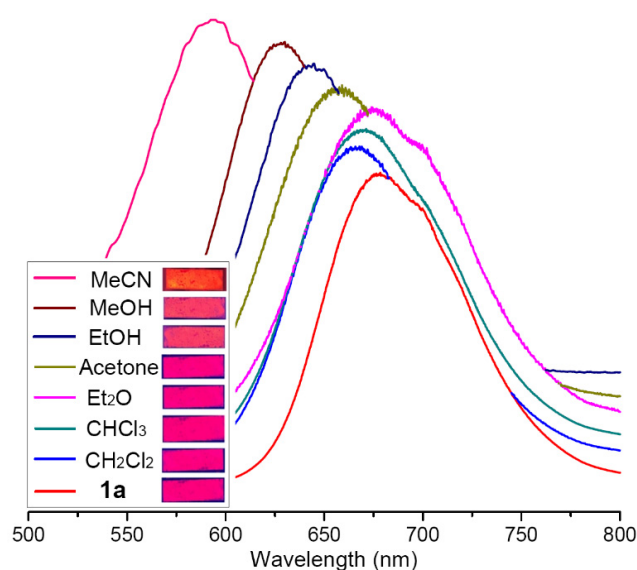


Figure 4. Emission spectra of **1a** and **1a** on exposure to different VOC vapors upon excitation at 400 nm. Photos of the powdered **1a** and **1a** (coating on a quartz slice) on exposure to different VOC vapors under 365 nm excitation (inset).

Complex **1a** was relatively stable toward air and moisture. The emission of **1a** shifted to 718 nm when its powder was immersed in liquid water for 20 h (Figure S6). We suggested this red-shift was caused by the interaction between the $\text{Ag}_{10}\text{Cu}_6$ cluster center and water molecules. This interaction was weak and lessened when the content of water was decreased. Therefore, a low-energy shoulder could be observed at the emission curve of **1a**, which indicated that a little portion of **1a** was hydrated by moisture when it was put in open air for days.

The emission of **1a** changed when this cluster was exposed to other VOC vapors. The less-coordinating VOC molecules, such as CH_2Cl_2 , CHCl_3 and Et_2O , caused only minor blue-shifting ($\lambda_{\text{max}} = 666, 671$ and 670 nm, respectively), whereas those VOCs with stronger donor groups, including acetone ($\text{C}=\text{O}$), MeOH ($-\text{OH}$) and MeCN ($-\text{CN}$), caused obvious blue-shifted emissions with $\lambda_{\text{max}} = 658$ nm (acetone), 628 nm (MeOH) and 594 nm (MeCN), respectively. The changes in emission wavelength on exposure of **1a** to MeOH and MeCN were 50 nm and 84 nm, respectively, which is visible to the naked eye under 365 nm LED irradiation (Figure 4).

2.3. Photoluminescent Probe for the Detection of MeCN

The significant vapor-chromic response of **1a** encouraged us to prepare a PL sensing film by compositing **1a** with PMMA (3% *w/w*). This film showed a visible red-to-orange PL change on exposure to a saturated atmosphere of MeCN vapor (Figure 5). The red emission could be recovered upon heating in air at 100 °C. This color interconversion was repeatable, giving a reusable PL probe for the detection of VOCs.

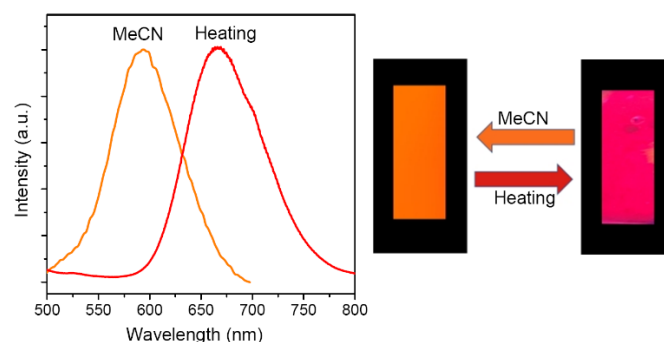


Figure 5. Emission spectra (left, Ex = 400 nm) and photos (right, under 365 nm UV light) of **1a**/PMMA film in MeCN vapor and heating to 100 °C.

3. Materials and Methods

3.1. Materials and Measurements

Bdppeda [37,38] and $\text{AgC}\equiv\text{CPh}$ [39] were prepared by literature procedures. $[\text{Cu}(\text{MeCN})_4](\text{ClO}_4)$ was commercially available. Elemental analyses (C, H and N) were performed on a Carlo Erba CHNO-S microanalyzer. PXRD measurements were recorded on a Bruker D2 Phaser X-ray diffractometer with a $\text{Cu K}\alpha$ source (30 kV, 10 mA). IR spectra were obtained on a VERTEX 70 FT-IR spectrometer ($4000\text{--}500\text{ cm}^{-1}$) with an ATR probe. Thermogravimetric analysis (TGA) was completed on a TA SDT-600 analyzer under an N_2 atmosphere in the range from room temperature to 900 °C, with a temperature heating rate of 10 °C/min. PL measurements were performed on an Edinburgh FLS1000 spectrophotometer. Positive-ion electrospray ion mass spectrometry (ESI-MS) was recorded on a Bruker microTOF-Q III mass spectrometer using MeOH as the mobile phase.

3.2. Synthesis of **1** and **1a**

A mixture containing bdppeda (46 mg, 0.1 mmol), $[\text{Cu}(\text{MeCN})_4](\text{ClO}_4)$ (131 mg, 0.4 mmol), 5 mL of CH_2Cl_2 and 5 mL of EtOH was stirred for 0.5 h at ambient temperature. $\text{AgC}\equiv\text{CPh}$ (84 mg, 0.4 mmol) was added into the resulting colorless solution and stirred for 3 h. The mixture turned red and was subsequently centrifuged. The supernatant was

diffused with Et₂O and afforded red crystals of 1·2CH₂Cl₂ after 1 day. The CH₂Cl₂ solvate escaped quickly in air, leaving **1** within an hour. Yield for **1**: 117 mg (73% based on Ag). Anal. Calcd for C₁₅₈H₁₃₂Ag₁₀Cl₄Cu₆N₄O₁₈P₄: C, 46.28; H, 3.24; N, 1.37. Found: C, 45.82; H, 3.34; N, 1.26. IR (ATR, cm⁻¹): 3419 (w), 3059 (w), 2019 (m), 1483 (m), 1435 (m), 1082 (vs), 750 (s), 687 (vs), 619(s).

Complex **1** was placed in a vacuum oven at 120 °C for 1 h and produced **1a** on cooling to room temperature. The yield was almost quantitative.

3.3. Preparation of **1a**/PMMA

A 9 mg sample of **1a** was carefully ground in a mortar and pestle, dispersed in PMMA/toluene solution (20% w/w, 1.5 g) and sonicated for 30 min. The mixture was applied to glass slides (3 × 6 cm²) and left to dry in air over several hours. The dried film was removed from the slide and cut into small pieces (1.5 × 4 cm²).

3.4. Single-Crystal Crystallography

A single crystal of 1·2CH₂Cl₂ was collected from the above synthesis. SCXRD analysis was performed on a Bruker D8 Venture diffractometer using graphite-monochromated Ga K α ($\lambda = 1.34138 \text{ \AA}$) radiation at 120 K. All data were integrated with Bruker SAINT and a multi-scan absorption correction was applied. The structure was solved by direct methods using SHELXS 2016/6 (Sheldrick, 2016) and refined by full-matrix least-squares methods against F^2 by SHELXL-2016/6 (Sheldrick, 2016) [40]. All non-hydrogen atoms were refined anisotropically. The hydrogen atoms of the -OH groups of EtOH were first located from a Fourier map and then refined to ride on the O atoms. All other hydrogen atoms were added in idealized positions and constrained to ride on their parent atoms. The data were deposited to the Cambridge Crystallographic Data Centre (CCDC number 2226387). A summary of the key crystallographic data is given in Table 1. Selected bond lengths and angles are listed in Table S1.

Table 1. Selected crystallographic data and refinement parameters for 1·2CH₂Cl₂.

Compound	1·2CH ₂ Cl ₂
Empirical formula	C ₁₆₀ H ₁₃₆ Ag ₁₀ Cl ₈ Cu ₆ N ₄ O ₁₈ P ₄
Formula weight	4270.14
Crystal system	monoclinic
Space group	<i>P</i> 21/ <i>n</i>
<i>a</i> /Å	30.834(2)
<i>b</i> /Å	16.5897(11)
<i>c</i> /Å	33.5688(19)
β /°	116.652(2)
<i>V</i> /Å ³	15,346.8(17)
<i>Z</i>	4
ρ_{calc} /g·cm ⁻³	1.848
μ /mm ⁻¹	12.665
<i>F</i> (000)	8432
θ_{max} /°	56.966
No. of reflections measured	345,696
No. of independent reflections	31,366 ($R_{\text{int}} = 0.1724$)
Data/restraints/parameters	31,366/79/1867
R_1 [$I > 2.00 \sigma(I)$] ^a	0.1049
wR_2 (all reflections)	0.3419
Goodness of fit	1.209

^a $R_1 = \sum ||F_o| - |F_c|| / \sum |F_o|$, $wR_2 = \{\sum w(F_o^2 - F_c^2)^2 / \sum w(F_o^2)^2\}^{1/2}$, $\text{GOF} = \{\sum w((F_o^2 - F_c^2)^2) / (n - p)\}^{1/2}$, where n = number of reflections and p = total number of parameters refined.

4. Conclusions

An Ag₁₀Cu₆ cluster **1** stabilized by PNNP ligand bdppthi and C≡CPh anions was prepared. The two Cu ends of the Ag₁₀Cu₆ core were coordinated with EtOH molecules.

Removing these solvates from **1** by vacuum heating produced **1a**, which could be restored to **1** by exposure to EtOH vapor. The maximum PL emission of **1** at 644 nm shifted to 678 nm when converted to **1a**. This reversible vapor-chromic response also occurred with other VOCs, particularly those with polar functional groups such as MeCN and MeOH, which exhibited the largest blue-shift of emissions up to 50 and 84 nm, respectively. A reusable chromic PL probe containing 3% (*w/w*) **1a** in PMMA exhibited a visible red-to-orange emission change when exposed to MeCN vapor.

Supplementary Materials: The following supporting information can be downloaded at: <https://www.mdpi.com/article/10.3390/molecules28031257/s1>, Figure S1: IR spectra of **1** and **1a**; Figure S2: Experimental and simulated isotopic patterns in the positive ion ESI-MS spectra of **1** in MeOH; Figure S3: TGA curve of **1** in a N₂ stream; Figure S4: Emission of **1a** over four cycles of exposure to EtOH vapor and vacuum heating; Figure S5: PXRD patterns of as-synthesized **1a**, **1a** after four EtOH exposure/elimination cycles and being left in air for another 1 month; Figure S6: Emission spectra of **1a** in air and its powder after immersed in water for 20 h.; Table S1: Selected bond lengths and angles for **1**·2CH₂Cl₂.

Author Contributions: W.Y., S.H., Y.W., S.Y. and X.-Q.C. conceived the study; Z.-G.R., H.-X.L. and D.J.Y. drafted the manuscript; Z.-G.R., W.Y. and Y.W. prepared the figures. All authors have read and agreed to the published version of the manuscript.

Funding: This work was financially supported by the Suzhou Science and Technology Plan Project (Grant No. SGC2021016) and the National Natural Science Foundation of China (Grant No. 21671144).

Institutional Review Board Statement: Not applicable.

Informed Consent Statement: Not applicable.

Data Availability Statement: The crystallographic data are available from the Cambridge Crystallographic Data Centre (CCDC). Other data not presented in the Supplementary Materials are available on request from the corresponding author.

Conflicts of Interest: The authors declare no conflict of interest.

References

1. Wenger, O.S. Vapochromism in organometallic and coordination complexes: Chemical sensors for volatile organic compounds. *Chem. Rev.* **2013**, *113*, 3686–3733. [[CrossRef](#)] [[PubMed](#)]
2. Lin, H.; Jang, M.; Suslick, K.S. Preoxidation for colorimetric sensor array detection of VOCs. *J. Am. Chem. Soc.* **2011**, *133*, 16786–16789. [[CrossRef](#)] [[PubMed](#)]
3. Prodi, L.; Bolletta, F.; Montalti, M.; Zaccheroni, N. Luminescent chemosensors for transition metal ions. *Coord. Chem. Rev.* **2000**, *205*, 59–83. [[CrossRef](#)]
4. Zhang, X.; Li, B.; Chen, Z.H.; Chen, Z.N. Luminescence vapochromism in solid materials based on metal complexes for detection of volatile organic compounds (VOCs). *Mater. Chem.* **2012**, *22*, 11427–11441. [[CrossRef](#)]
5. Li, E.; Jie, K.; Liu, M.; Sheng, X.; Zhu, W.; Huang, F. Vapochromic crystals: Understanding vapochromism from the perspective of crystal engineering. *Chem. Soc. Rev.* **2020**, *49*, 1517–1544.
6. Krytchankou, I.S.; Koshevoy, I.O.; Gurzhiy, V.V.; Pomogaev, V.A.; Tunik, S.P. Luminescence solvato- and vapochromism of alkynyl-phosphine copper clusters. *Inorg. Chem.* **2015**, *54*, 8288–8297. [[CrossRef](#)] [[PubMed](#)]
7. Jin, M.; Sumitani, T.; Sato, H.; Seki, T.; Ito, H. Mechanical-stimulation-triggered and solvent-vapor-induced reverse single-crystal-to-single-crystal phase transitions with alterations of the luminescence color. *J. Am. Chem. Soc.* **2018**, *140*, 2875–2879. [[CrossRef](#)]
8. England, K.R.; Lim, S.H.; Luong, L.M.C.; Olmstead, M.M.; Balch, A.L. Vapoluminescent behavior and the single-crystal-to-single-crystal transformations of chloroform solvates of [Au₂(μ-1,2-bis(diphenylarsino)ethane)₂](AsF₆)₂. *Chem. Eur. J.* **2019**, *25*, 874–878. [[CrossRef](#)]
9. Chu, A.; Hau, F.K.W.; Yao, L.Y.; Yam, V.W.W. Decanuclear gold(I) sulfido pseudopolymorphs displaying stimuli-responsive RGBY luminescence changes. *ACS Mater. Lett.* **2019**, *1*, 277–284. [[CrossRef](#)]
10. Artem'ev, A.V.; Davydova, M.P.; Berezin, A.S.; Ryzhikov, M.R.; Samsonenko, D.G. Dicopper(I) paddle-wheel complexes with thermally activated delayed fluorescence adjusted by ancillary ligands. *Inorg. Chem.* **2020**, *59*, 10699–10706. [[CrossRef](#)]
11. Smith, M.B. The backbone of success of P,N-hybrid ligands: Some recent developments. *Molecules* **2022**, *27*, 6293. [[PubMed](#)]
12. Baranov, A.Y.; Slavova, S.O.; Berezin, A.S.; Petrovskii, S.K.; Samsonenko, D.G.; Bagryanskaya, I.Y.; Fedin, V.P.; Grachova, E.V.; Artem'ev, A.V. Controllable synthesis and luminescence behavior of tetrahedral Au@Cu₄ and Au@Ag₄ clusters supported by tris(2-pyridyl)phosphine. *Inorg. Chem.* **2022**, *61*, 10925–10933. [[CrossRef](#)] [[PubMed](#)]

13. Huang, Q.; Zhang, R.; He, L.-H.; Chen, J.-L.; Zhano, F.; Liu, S.-J.; Wen, H.-R. Thermo-, mechano-, and vapochromic dinuclear cuprous-emissive complexes with a switchable CH₃CN–Cu bond. *Inorg. Chem.* **2022**, *61*, 15629–15637. [[CrossRef](#)]
14. Xu, L.J.; Zhang, X.; Wang, J.Y.; Chen, Z.N. High-efficiency solution-processed OLEDs based on cationic Ag₆Cu heteroheptanuclear cluster complexes with aromatic acetylides. *J. Mater. Chem. C* **2016**, *4*, 1787–1794. [[CrossRef](#)]
15. Chen, K.; Shearer, J.; Catalano, V.J. Subtle modulation of Cu₄X₄L₂ phosphine cluster cores leads to changes in luminescence. *Inorg. Chem.* **2015**, *54*, 6245–6256.
16. Wu, Y.; Wang, J.Y.; Zhang, L.Y.; Xu, L.J.; Chen, Z.N. Vapor-triggered green-to-yellow luminescence conversion due to the variation of ligand orientations in tetranuclear copper(I) complex. *Inorg. Chem.* **2020**, *59*, 17415–17420. [[CrossRef](#)] [[PubMed](#)]
17. Mizukami, S.; Houjou, H.; Sugaya, K.; Koyama, E.; Tokuhisa, H.; Sasaki, T.; Kanosato, M. Fluorescence color modulation by intramolecular and intermolecular π – π interactions in a helical zinc(II) complex. *Chem. Mater.* **2005**, *17*, 50–56. [[CrossRef](#)]
18. Kritchenkov, I.S.; Gitlina, A.Y.; Koshevoy, I.O.; Melnikov, A.S.; Tunik, S.P. Luminescent silver–copper “hourglass” hepta- and decanuclear alkynyl-phosphine clusters. *Eur. J. Inorg. Chem.* **2018**, *2018*, 3822–3828. [[CrossRef](#)]
19. Zhang, L.Y.; Xu, L.J.; Zhang, X.; Wang, J.Y.; Li, J.; Chen, Z.N. Spectroscopic and phosphorescent modulation in triphosphine-supported PtAg₂ heterotrinnuclear alkynyl complexes. *Inorg. Chem.* **2013**, *52*, 5167–5175.
20. Laguna, A.; Lasanta, T.; López-de-Luzuriaga, J.M.; Monge, M.; Naumov, P.; Olmos, M.E. Combining aurophilic interactions and halogen bonding to control the luminescence from bimetallic gold–silver clusters. *J. Am. Chem. Soc.* **2010**, *132*, 456–457. [[CrossRef](#)]
21. Mo, L.Q.; Jia, J.H.; Sun, L.J.; Wang, Q.M. Solvent-induced intercluster rearrangements and the reversible luminescence responses in sulfide bridged gold(I)–silver(I) clusters. *Chem. Commun.* **2012**, *48*, 8691–8693.
22. Lei, Z.; Pei, X.L.; Jiang, Z.G.; Wang, Q.M. Cluster linker approach: Preparation of a luminescent porous framework with NbO topology by linking silver ions with gold(I) clusters. *Angew. Chem. Int. Ed.* **2014**, *53*, 12771–12775. [[CrossRef](#)] [[PubMed](#)]
23. Tzeng, B.C.; Lin, C.Y.; Hung, J.W.; Chen, S.Y.; Chang, A.H.H.; Lee, G.H. Solvent-induced luminescence and structural transformation of a dinuclear gold(I) (aza-18-crown-6)dithiocarbamate compound. *Inorg. Chem.* **2021**, *60*, 2694–2703. [[CrossRef](#)] [[PubMed](#)]
24. Luong, L.M.C.; Olmstead, M.M.; Balch, A.L. A non-luminescent polymorph of [(cyclohexyl isocyanide)₂Au]PF₆ that becomes luminescent upon grinding or exposure to dichloromethane vapor. *Chem. Commun.* **2021**, *57*, 793–796. [[CrossRef](#)] [[PubMed](#)]
25. Jiang, B.; Zhang, J.; Ma, J.Q.; Zheng, W.; Chen, L.J.; Sun, B.; Li, C.; Hu, B.W.; Tan, H.; Li, X.; et al. Vapochromic behavior of a chair-shaped supramolecular metallacycle with ultra-stability. *J. Am. Chem. Soc.* **2016**, *138*, 738–741. [[CrossRef](#)] [[PubMed](#)]
26. Hudson, Z.M.; Sun, C.; Harris, K.J.; Lucier, B.E.G.; Schurko, R.W.; Wang, S. Probing the structural origins of vapochromism of a triarylboron-functionalized platinum(II) acetylide by optical and multinuclear solid-state NMR spectroscopy. *Inorg. Chem.* **2011**, *50*, 3447–3457.
27. Nayeri, S.; Jamali, S.; Jamjah, A.; Samouei, H. Tetranuclear Au₂Cu₂ clusters with butterfly- and planar-shaped metal cores: Strong rigidochromism induced by Jahn–Teller distortion in two-coordinated gold(I) centers. *Inorg. Chem.* **2019**, *58*, 12122–12131.
28. López-de-Luzuriaga, J.M.; Monge, M.; Olmos, M.E.; Quintana, J.; Rodríguez-Castillo, M. Stimuli-responsive solvatochromic Au(I)–Ag(I) clusters: Reactivity and photophysical properties induced by the nature of the solvent. *Inorg. Chem.* **2019**, *58*, 1501–1512. [[CrossRef](#)]
29. Strasser, C.E.; Catalano, V.J. “On–off” Au(I)···Cu(I) interactions in an Au(NHC)₂ luminescent vapochromic sensor. *J. Am. Chem. Soc.* **2010**, *132*, 10009–10011.
30. Li, Y.J.; Deng, Z.Y.; Xu, X.F.; Wu, H.B.; Cao, Z.X.; Wang, Q.M. Methanol triggered ligand flip isomerization in a binuclear copper(I) complex and the luminescence response. *Chem. Commun.* **2011**, *47*, 9179–9181.
31. Lee, J.Y.; Kim, H.J.; Jung, J.H.; Sim, W.; Lee, S.S. Networking of calixcrowns: From heteronuclear endo/exocyclic coordination polymers to a photoluminescence switch. *J. Am. Chem. Soc.* **2008**, *130*, 13838–13839. [[CrossRef](#)]
32. Wang, Y.; Shi, Y.; Zou, X.; He, Y.; Wang, X. Pyridylphosphine supported Ag(I) and Cu(I) complexes for detection of alcohols and nitriles via structural transformations from 1D to 0D. *CrystEngComm* **2019**, *21*, 5595–5601.
33. Lei, Z.; Chang, S.S.; Wang, Q.M. Vapochromic gold(I)–silver(I) cluster protected by alkynyl and phosphine ligands. *Eur. J. Inorg. Chem.* **2017**, *2017*, 5098–5102. [[CrossRef](#)]
34. Wang, Y.; Yan, J.J.; Hu, S.; Young, D.J.; Li, H.X.; Ren, Z.G. A photoluminescent Ag₁₀Cu₆ cluster stabilized by a PNNP ligand and phenylacetylides selectively and reversibly senses ammonia in air and water. *Chem. Asian J.* **2021**, *16*, 2681–2686. [[CrossRef](#)] [[PubMed](#)]
35. Sun, S.; Ren, Z.G.; Yang, J.H.; He, R.T.; Wang, F.; Wu, X.Y.; Gong, W.J.; Li, H.X.; Lang, J.P. Formation of N-heterocyclic Biphosphine Ligands from Ag(I)-Assisted Condensation Reactions between bdppeda and Formaldehyde and Their Binuclear Silver(I) Complexes. *Dalton Trans.* **2012**, *41*, 8447–8454. [[CrossRef](#)] [[PubMed](#)]
36. Bondi, A. Van der Waals volumes and radii. *J. Phys. Chem.* **1964**, *68*, 441–451. [[CrossRef](#)]
37. Zhang, J.; Vittal, J.J.; Henderson, W.; Wheaton, J.R.; Hall, I.H.; Hor, T.S.A.; Yan, Y.K. Tricarbonylrhenium(I) complexes of phosphine-derivatized amines, amino acids and a model peptide: Structures, solution behavior and cytotoxicity. *J. Organomet. Chem.* **2002**, *650*, 123–132. [[CrossRef](#)]
38. Grim, S.O.; Matienzo, L.J. The synthesis and characterization of some novel polydentate phosphorus-nitrogen ligands. *Tetrahedron Lett.* **1973**, *14*, 2951–2953. [[CrossRef](#)]

39. Teo, K.; Xu, Y.H.; Zhong, B.Y.; He, Y.K.; Chen, H.Y.; Qian, W.; Deng, Y.J.; Zou, Y.H. A comparative study of third-order nonlinear optical properties of silver phenylacetylide and related compounds via ultrafast optical Kerr effect measurements. *Inorg. Chem.* **2001**, *40*, 6794–6801.
40. Sheldrick, G.M. *SHELXTL-2016/6*; Universität Göttingen: Göttingen, Germany, 2016.

Disclaimer/Publisher's Note: The statements, opinions and data contained in all publications are solely those of the individual author(s) and contributor(s) and not of MDPI and/or the editor(s). MDPI and/or the editor(s) disclaim responsibility for any injury to people or property resulting from any ideas, methods, instructions or products referred to in the content.